Tribological Effects of 0.30% Titanium in Nickel Aluminium Bronze Alloy Post-casting, Heat Treatment and Forging

Emad ELWAHAB [1], Ismail ESEN [1], Hayrettin AHLATCI [2], Esma KESKIN [3], Volkan KARAKURT [4]

[1] *Mechanical Engineering Department, Karabuk University, Karabuk 78050, Turkey*
[2] *Metallurgical and Materials Engineering Department, Karabuk University, Karabuk 78050, Turkey*
[3] *BUMA Engineering and Consulting Inc., Ankara, 6980, Turkey*
[4] *Saglam Metal Industry Trade Inc. R and D Center, İstanbul, Turkey*

http://doi.org/10.5755/j02.ms.41241

Received 22 April 2025; accepted 4 August 2025

This study explores the effects of solution treatment, tempering, and forging on the microstructure and tribological properties of 0.30 % Ti-alloyed nickel-aluminum bronze. The modified NAB alloy exhibited a refined microstructure comprising a copper-rich α-phase, martensitic β-phase, and various intermetallic κ (kappa) phases. Titanium addition enhanced nucleation during solidification, reduced dendritic arm spacing, and promoted the formation of discrete κ phases, thereby improving grain refinement and phase uniformity. Notably, tempering the β-phase facilitated its partial decomposition into α and κ_{III}, with further precipitation of κ_{IV} and κ_{II} phases. Forging significantly altered the alloy's morphology, fragmenting dendritic arms into near-spherical forms and increasing the formation of secondary κ_{IV} phases while preserving the fundamental α, β, and κ phases. Hardness analysis revealed that Ti addition markedly improved hardness, with NAB-0.30 %Ti achieving 239.53 HB and 254.06 HB after heat treatment and forging, respectively. Enhanced hardness and improved wear resistance have been attributed to the presence of intermetallic κ phases, increased dislocation density, and grain refinement. Tribological testing confirmed that the forged NAB-0.30 %Ti alloy demonstrated the lowest friction coefficient (0.097), minimal weight loss (0.0035 g), and the best wear rate (1.17×10^{-8} g/N·m) over 10,000 meters of sliding distance. The findings highlight titanium's role in refining microstructure and enhancing both hardness and tribological performance of NAB, making it a promising candidate for applications demanding superior wear resistance.

Keywords: nickel-aluminum bronze, titanium, heat treatment, forging process, tribological behaviour.

1. INTRODUCTION

The creation of nickel aluminium bronze (NAB) alloys is a multifaceted process that necessitates the meticulous selection of alloying elements, casting methods, and thermal treatments. NAB is predominantly sourced from a binary copper-aluminium system, supplemented with nickel and iron to improve its mechanical characteristics and corrosion resistance. NAB alloys generally comprise 9 – 12 % aluminium, with variable quantities of nickel (up to 6 %) and iron, which enhance the alloy`s performance in maritime applications [1 – 8]. The standard as-cast microstructure comprises a ductile, copper-rich α phase, a rigid martensitic β (beta) phase, and several intermetallic κ (kappa) phases, collectively endowing the alloy with its advantageous mechanical properties [5, 9 – 13]. The solidification temperature of NAB is approximately 1070 °C, and the cooling pace can considerably influence the resultant microstructure and, subsequently, the mechanical properties of the alloy [13, 14]. Moreover, the incorporation of nickel and iron not only augments corrosion resistance but also improves the mechanical strength and tribological characteristics of the alloy, rendering it appropriate for high-stress applications [12, 15 – 18]. These treatments can produce a tempered martensitic or bainitic microstructure, hence improving the alloy's strength and ductility [5, 13].

Modifying the microstructure via thermal treatments is crucial for attaining the optimal combination of strength and corrosion resistance, especially in demanding maritime settings [4, 19]. The wear characteristics of NAB are markedly affected by its microstructural phases, comprising α (alpha), β, and several intermetallic phases. The intricate interaction of these phases dictates the mechanical properties and wear resistance of the alloy, rendering it essential to comprehend their influence on wear performance. The β phase, particularly the retained β' phase, is a tougher, martensitic structure that improves the alloy's wear resistance. The mechanical characteristics and abrasive behaviour of NAB are significantly influenced by their microstructure, with the hard β phase enhancing strength and wear resistance [12, 20]. Research indicates that the existence of this phase markedly enhances mechanical qualities, such as tensile strength and hardness, rendering it more appropriate for applications where wear resistance is essential [5, 11, 12, 21, 22]. Elevated nickel levels correlate with a decrease in the proportion of β and γ_2 phases, facilitating the emergence of κ phases that enhance the alloy's hardness and wear resistance [9, 20]. The κ phases are generally more resilient than the α phase and can

* Corresponding author: E. Elwahab
E-mail: *eoelwahab@elmergib.edu.ly*

enhance the alloy's performance under abrasive conditions [9, 12].

Heat treatment procedures, including quenching and aging, can alter the microstructure, thereby increasing the hardness and strength of the alloy, while potentially diminishing ductility [13, 20]. The microstructural evolution during these treatments can result in the development of a tempered martensitic structure, recognized for enhancing wear resistance [13]. The microstructural attributes of NAB alloys, affected by heat treatment and processing techniques, are crucial in influencing their wear performance [4, 10, 23]. Heat treatment techniques can enhance the microstructure, hence increasing the wear properties of NAB alloys during sliding contact with other materials [5, 24]. The existence of several phases inside the alloy enhances its strength and toughness, which are crucial for applications demanding high performance under mechanical stress [11, 22]. The mechanical strength of NAB alloys can be augmented using diverse processing techniques, such as heat treatment and friction stir processing, which refine the microstructure and enhance hardness and tensile strength [20, 22]. Furthermore, the tribological properties of NAB alloys demonstrate that they sustain their performance despite exposure to corrosive conditions, rendering them suitable for underwater applications [15, 25 – 30].

The incorporation of titanium into nickel-aluminium bronze markedly improves its microstructural properties and wear resistance. The enhancement of the microstructure, stabilization of advantageous phases, and augmentation of mechanical properties jointly enhance the alloy`s performance in wear-intensive applications. The selection of 0.3 % titanium (Ti) in materials studies has likely been informed by various factors, including the formation of solid solutions, enhancements in mechanical properties, and the microstructural implications associated with different concentrations of Ti. The initial introduction of Ti into a tungsten (W) matrix, as noted by Sun et al., [31] suggests that the replacement of W atoms by larger Ti atoms results in significant lattice distortion, contributing to enhanced hardness through the generation of elastic strain fields. Ti's ability to strengthen thin films through such mechanisms forms a foundational understanding for why specific percentages, such as 0.3 %, may have been chosen; this concentration could facilitate a balance between enhanced mechanical performance and modifiable microstructural properties.

2. MATERIALS AND METHODS

Sample manufacturing casting trials were done at Saglam Metal Industry and Trade's R&D Centre. Manufacturing criteria were followed to purchase a nickel aluminium bronze ingot for casting trials. Industrial ingots were the main material, but laboratory-specific materials were produced. The casting testing ingot was made from pure copper scrap, aluminium, iron, and nickel utilizing permanent mold casting. The melting process used a 300-kilogram induction furnace. The prefabricated nickel aluminium bronze ingot was sectioned and melted. The CuLi permalloy removed oxygen from the liquid metal, whereas the 30 % copper titanium permalloy added titanium. Copper lithium pre-alloy removes gases after melting nickel aluminium bronze. Two charges were generated: one titanium-free and one titanium-0.30 %. Before casting, a 30 % copper titanium permalloy was added to the molten metal during the last melting phase. Castings were done at 1230 ℃. Table 1 shows the chemical makeup of NAB and NAB-0.30 % Ti alloys. The industrial ingot's chemical composition was measured with an Oxford optical emission spectrometer at the casting site. Japan's Rigaku Ultima IV X-ray diffraction instrument revealed the alloy's phases. The scanning range was 10 – 90 degrees at 3 degrees per minute. The casting samples were heat treated after solution treatment (S.T.) at 875°C for 90 minutes and tempering (T.) at 650 °C for 2 hours.

Table 1. Alloy weight percentages

Alloy	Chemical composition, wt.%					
	Al	Fe	Ni	Mn	Ti	Cu
NAB	10.19	3.01	4.41	0.31	–	Bal.
NAB-0.30 % Ti	9.95	2.99	4.28	0.30	0.30	Bal.

Open-die forging was performed using a ram, rotating the alloy around its axis with an industrial hammer. The temperature was controlled with a laser thermocouple. According to the literature, optimum strength values were achieved at 870 °C [8], and 80 % deformation [7]. To accomplish this, cylindrical metal rods with a diameter of 68 mm were forged to produce rods with a square cross-sectional area of 27 × 27 mm.

After heat treatment and forging processes, NAB and NAB-0.30 % Ti samples were cut into 10 × 20 × 10 mm pieces using a water-cooled band saw. The samples were sanded and polished with Microtext automated equipment after cutting. The sanding process used 320, 400, 600, 800, 1000, and 2500 grits. After sanding, a 3 μm Al_20_3 liquid solution was used for polishing. The etching process used 5 grams $FeCl_3$, 50 millilitres HCl, and 100 millilitres of clean water. An LOM-Carl Zeiss light optical microscope was used to study phase structure grain changes. To find secondary phases, the SEM-Carl Zeiss Ultra Plus scanning electron microscope and EDX were used. The hardness of NAB and NAB-0.30 % Ti alloys was measured on the Brinell Hardness tester by applying a load of 187.5 N with 2.5 mm steel balls. Hardness measurements were performed by taking at least five consecutive successful measurements, and the mean and standard deviation of these measurements were calculated.

Tribological testing was done at ambient temperature with the loading axis parallel to the rolling direction. Wear testing used rectangular prism samples measuring 18 mm × 14 mm × 10 mm. Before abrasion tests, the surfaces were polished with 1200 μm sandpaper. After ethanol cleaning, the samples were weighed using a Precise scale with 0.1 mg accuracy. The reciprocating wear testing device was used to deliver a 20 N force, 0.1 m/s sliding velocity, and 10,000 m of abrasion tests in dry conditions. High-hardness AISI 52100 steel balls are used as abrasive tips. At 200 m intervals, ethanol cleaned the sample surface of worn debris. Before being reattached to the back-and-forth abrasion tester, each sample was cleaned with ethanol and weighed using calibrated scales. The beginning weight was subtracted from the final weight using this data to

determine the weight loss with distance. For every sample, the mean and standard deviation of the abrasion findings from a minimum of three tests were computed. Eq. 1 converted mass loss data into wear rate:

$$Wear\ Rate\ Per\ Unit\ Force\ (\mathrm{g}/(\mathrm{N}*\mathrm{m}) = \left(\frac{Mass\ Loss\ Due\ to\ Wear\ (g)}{Force\ Applied\ (N)*Displacement(m))}\right). \quad (1)$$

The coefficient of friction was measured using a load cell on the tribometer arm and recorded in real time on the computer. SEM and EDX were used to assess alloy element concentration and applied stress during the wear test.

3. RESULTS AND DISCUSSION

3.1. XRD patterns

XRD analysis is crucial in materials research because it provides information on crystallographic structure, phase composition, and microstructure. Materials characterisation, industrial quality control, and material development all benefit from XRD. Materials having complex compositions can be identified by XRD. The NAB alloy has improved wear resistance and ductility due to the inclusion of κ phases [32]. Fig. 1 XRD analyses indicated the existence of copper-rich $AlCu_4$ and α-Cu phases at the highest peak. Furthermore, the α-Cu phase was observed in the terminal peaks of all alloys. Fig. 1 demonstrates that the NAB alloy has AlNi and $AlFe_3$ phases at an angle of 30.95°. The NAB-0.30 %Ti alloy demonstrated the presence of the AlTi phase at an angle of 21.90°, signifying the existence of titanium. Consequently, the $AlFe_3$ phase was observed at an angle of 27.25°. According to the NAB phase equilibrium diagram [33], 10 % Al content in NAB alloy led to the formation of κ phase containing Fe and Ni.

3.2. Microstructure

LOM pictures of NAB and NAB-0.30 % Ti alloys after solution treatment and tempering post-casting are shown in Fig. 2 shows post-forging LOM pictures of the investigated alloys. The addition of grain-refining elements such as Ti to the alloy increases the grain formation rate before the proliferation of nuclei, which contributes to grain refinement.

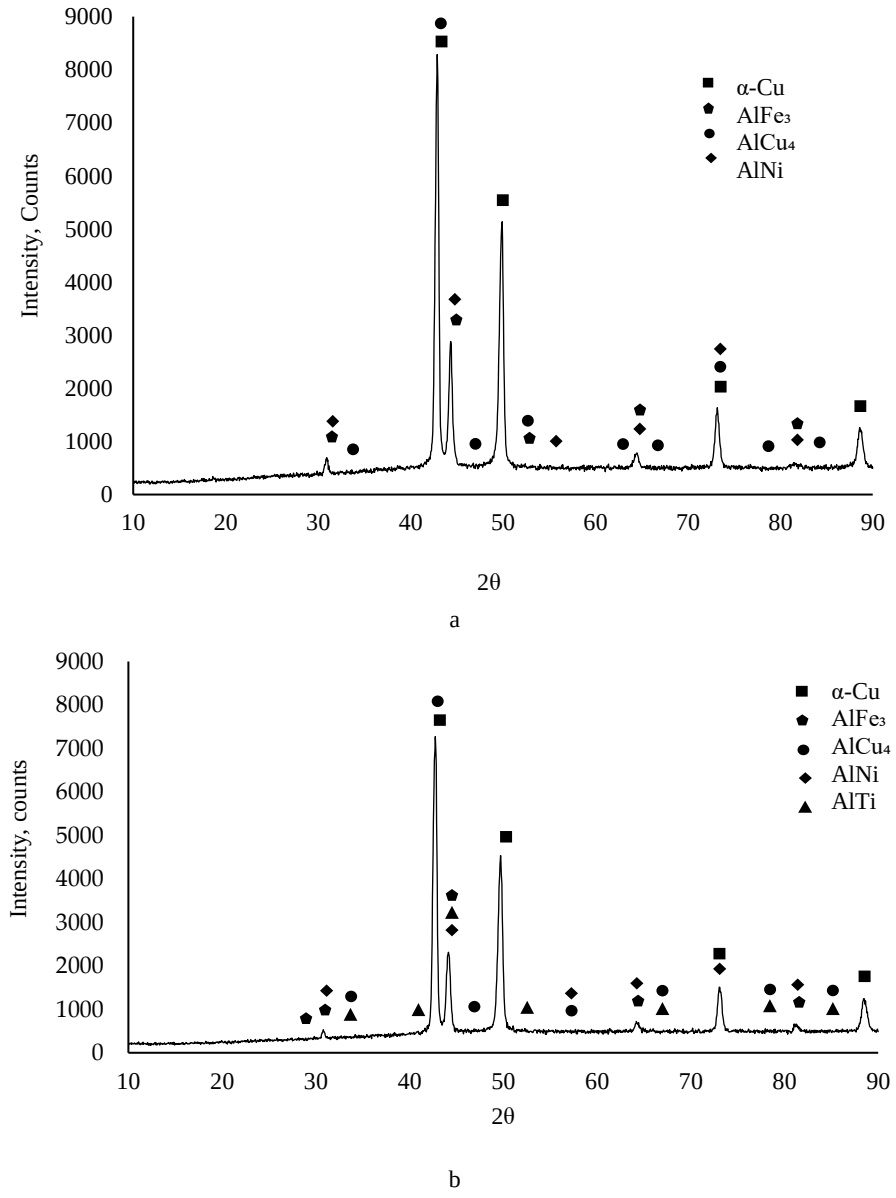

Fig. 1. X-ray diffraction patterns: a – NAB; b – NAB with 0.30 % titanium

A higher number of nucleation sites per unit volume leads to the formation of smaller grains [34]. Titanium increases nucleation sites, resulting in smaller grains, which refines grain structure. In several studies on nickel-bearing aluminium bronze, the heat-treated NAB alloy microstructure in Fig. 2 a is typical. NAB has proven the occurrence of copper-rich α solid solution phase, martensitic *β* phase, and several intermetallic κ phases, such as leaf-shaped κ_I, thin κ_{III}, and black globular κ_{IV} [35 – 39]. Fig. 2 b shows that adding 0.30 % titanium to NAB alloys reduces dendritic arm thickness and increases κ phase abundance. Additionally, the tempered *β* phase showed significant κ_{IV} and κ_{II} precipitation. Tempering *β* may decompose martensitic *β* into small *α* and κ_{III} clumps. Fig. 2 shows that forging NAB and NAB-0.30%Ti alloys reduced microstructure thickness. After forging, the alloys maintained the same *α*, *β*, and κ phases (Fig. 2 c and d). Forging fractured and shaped dendritic arms into approximately spherical forms. The forging process added κ_{IV} steps. The addition of 0.30 %Ti to NAB alloys resulted in the formation of κ_I and κ_{III} phases.

Fig. 3 a and b shows SEM images of NAB and NAB-0.30 %Ti alloys after solution treatment (S.T.) and tempering (T) post-casting. In contrast, Fig. 3 c and d shows SEM pictures of the identical alloys after forging. Table 2 shows the second phase EDX analysis findings, which show diverse morphologies (1-8) in Fig. 3. The SEM pictures reveal the alloys' microstructure, including α, β, and intermetallic κ phases. The α phase has a high copper content, whereas the retained β phase has a tempered structure and concentrated AlNi precipitates.

Table 2. EDX weight percentages of the marked numbers in Fig. 3

	Points	Al	Ti	Mn	Fe	Ni	Cu
Fig. 3 a and b	1	5.35	–	0.47	11.14	5.70	77.35
	2	4.79	–	0.88	1.08	4.17	89.08
	3	5.91	–	0.25	0.58	4.84	88.42
	4	6.11	–	0.87	0.80	5.22	87.01
	5	5.27	9.57	0.61	18.96	6.47	59.14
	6	2.92	5.19	0.37	12.11	5.51	73.93
	7	16.16	4.13	0.41	0.09	4.75	74.46
	8	6.89	3.95	0.45	0.26	4.95	83.49
Fig. 3 c and d	1	8.27	–	0.10	0.81	5.60	85.22
	2	7.30	–	0.03	0.72	5.01	86.95
	3	4.37	–	–	0.32	5.41	89.91
	4	6.65	–	0.43	0.22	5.77	86.93
	5	1.45	26.12	0.40	11.33	4.83	55.88
	6	9.79	6.66	–	12.70	9.13	61.72
	7	6.99	8.31	0.11	0.51	6.41	77.67
	8	6.81	5.16	–	1.14	6.37	80.53

Three separate κ phases have diverse morphologies and distributions. The κ_I phase, with significant iron concentration, is located within the α phase matrix, which has a rosette-shaped morphology. The κ_{IV} phase, located at the *α*-*β* boundary, has a spherical shape. The κ_{IV} phase is far more advanced than the κ_I phase.

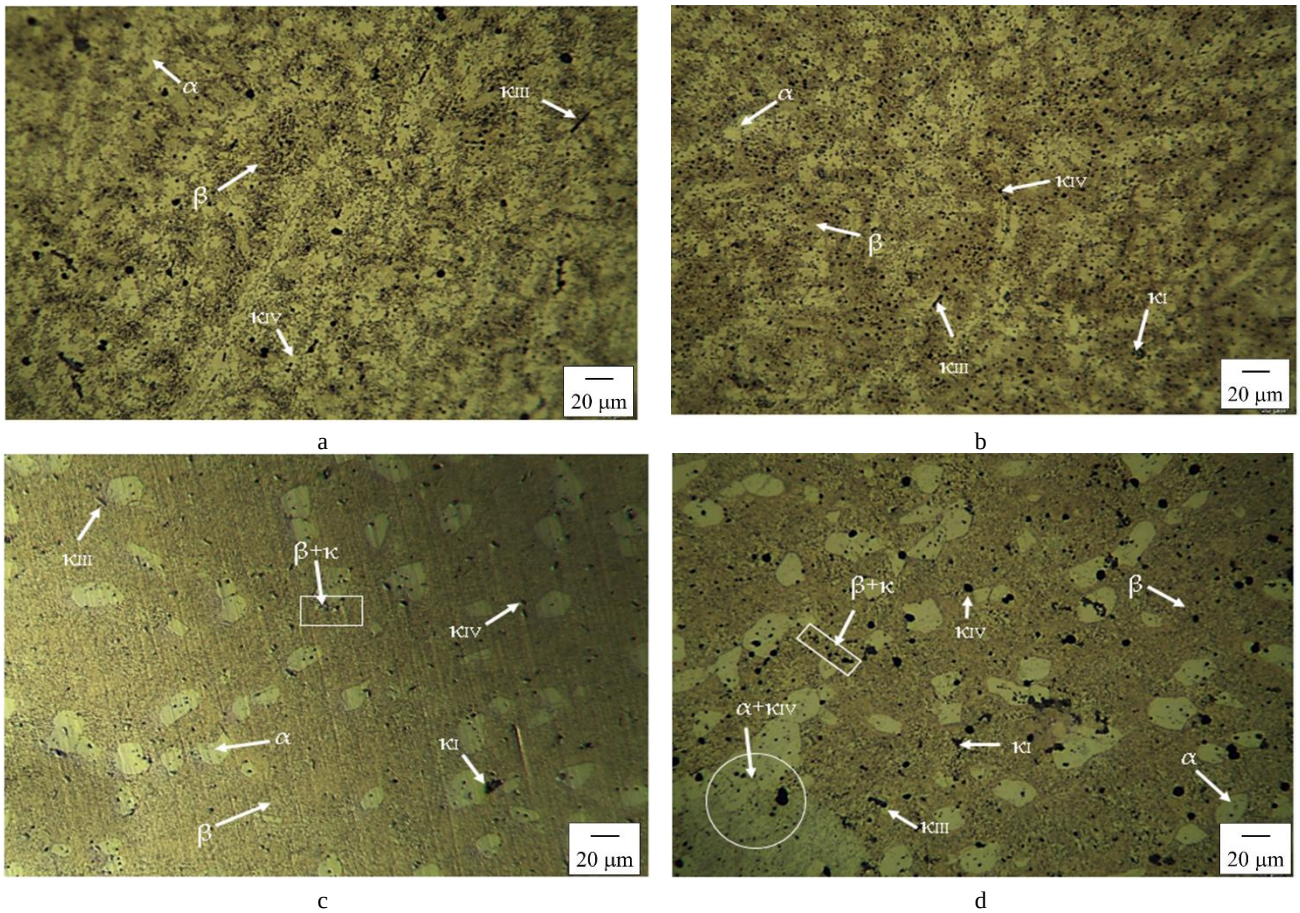

Fig. 2. LOM images after S.T. + T.: a – NAB; b – NAB-0.30 %Ti; c – NAB after F; d – NAB-0.30 %Ti after F

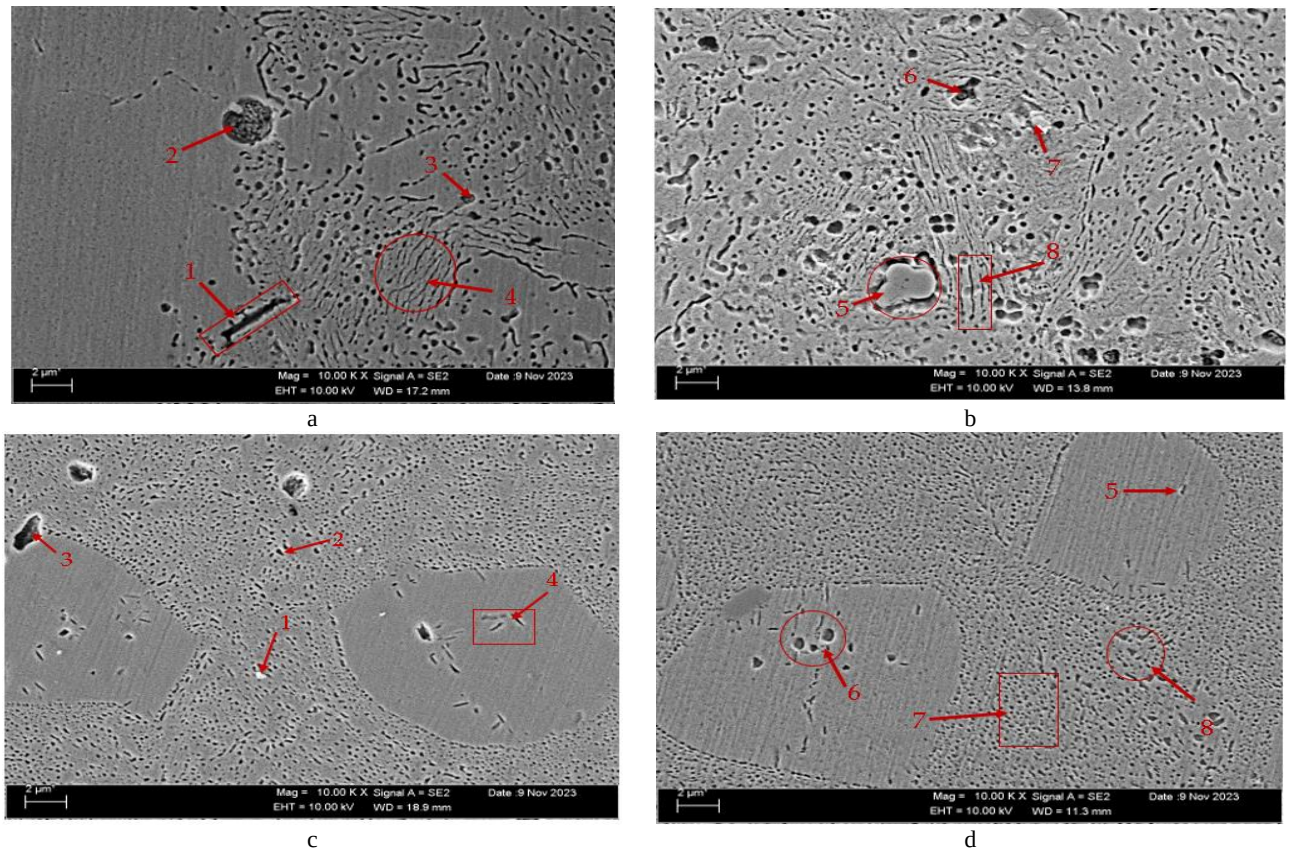

Fig. 3. SEM images after S.T. + T.: a – NAB; b – NAB-0.30 %Ti; c – NAB after F; d – NAB-0.30 %Ti after F

The lamellar κ_{III} phase, with high nickel content, is formed at the α and β inter-faces via eutectoid transformation of the β phase at low temperatures. The κ_{IV} phase, with higher iron content, is a refined precipitate within the α phase [39 – 41].

3.3. Hardness test results

Fig. 4 compares NAB and NAB-0.30 %Ti alloy hardness. The study includes post-solution treatment (S.T.) and tempering (T.) data for casting and forging.

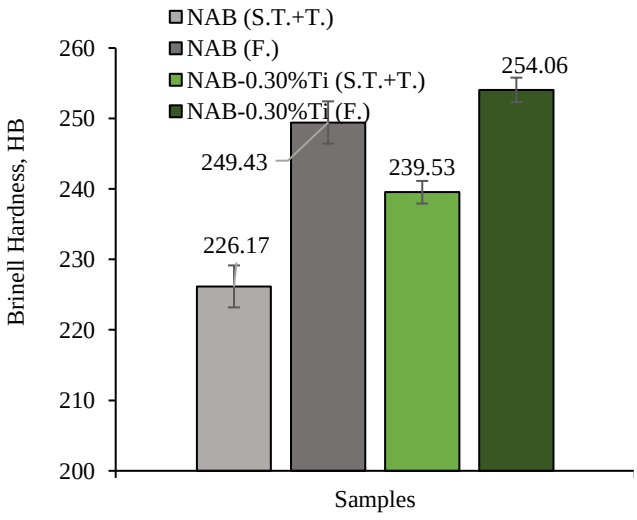

Fig. 4. Comparison of hardness between NAB and NAB-0.30 %Ti alloys

Forging increased the hardness of both alloys, but the NAB alloy without titanium had a lower hardness. After solution treatment (S.T.) and tempering (T) after casting and forging (F.), the NAB-0.30 %Ti alloy had the higher hardness values of 239.53 HB and 254.06 HB, respectively.Nickel-aluminium bronze's hardness comes from the complex interplay of its microstructure phases α, β, and κ. The martensitic features of the β phase increase hardness, whereas the intermetallic qualities of the κ phases increase strength. The κ phase, including intermetallic compounds after solidification, is essential for increasing NAB's hardness. The inclusion of κ phases can improve wear resistance and strength by creating a more complex microstructure [9, 12]. The κ phases' intermetallic properties increase the alloy's hardness, as they are harder than the α and β phases. The distribution and shape of κ phases can be influenced by alloying elements [6, 42]. Forging influences material hardness through grain refinement, phase transitions, and temperature changes during deformation. Heat treatment and forging have improved NAB's mechanical and tribological qualities such hardness, yield strength, and tensile strength. Nickel-aluminium bronze yield strength and tensile strength increase with hot forging at 850 °C, whereas elongation decreases. This is because microstructural refinement during forging increases dislocation density and grain structure, increasing hardness [43]. Alloying materials also impact NAB hardness [44]. Research shows that alloying compositions affect mechanical qualities like hardness [45]. Without titanium, NAB alloy hardness was lower than other alloys. Grain refinement is essential for alloy hardness.

Titanium grain refining reduces grain size and increases dislocation density, increasing hardness [46]. Grain refiners like titanium add solid particles to the alloy, increasing its hardness [46].

3.4. Tribological (wear) test results

Fig. 5 shows NAB and NAB-0.30 % Ti alloy weight decreases after solution treatment (S.T.) + tempering (T.) and forging (F.) while sliding at 0.1 m/s over 10,000 m. Fig. 6 a shows the determined wear rates of the aluminium alloys after this wear.

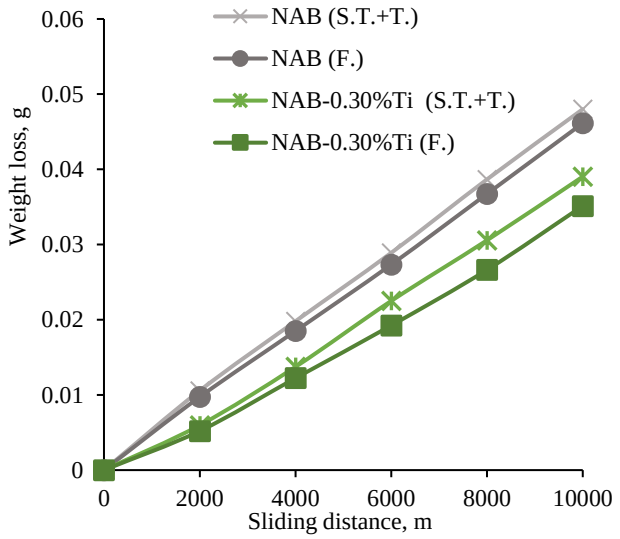

Fig. 5. Weight loss with wear of NAB and NAB-0.30 %Ti alloys

Fig. 6 b shows wear-related friction coefficients. In solution treatment (S.T.), tempering (T), and forging (F), the alloy with 0.30 % Ti had the best wear resistance. After forging (F.), the NAB-0.30 %Ti alloy showed 0.0035 g weight loss, 1.17×10^{-8} g/N·m wear rate, and 0.0970 friction coefficient after 10,000 m. Titanium makes NAB more resistant. Hardness and wear performance are important because tougher materials wear better and last longer under tough situations [49]. The presence and characteristics of nickel-aluminium bronze (NAB) κ phases significantly impact its wear behaviour. The κ phases, intermetallic compounds formed during alloying, significantly impact NAB's mechanical properties and wear resistance [19, 42]. The selective corrosion behaviour of κ phases may safeguard against wear in certain settings, extending the service life of NAB components. Heat treatment affects NAB's mechanical properties, particularly wear resistance. Heat treatments can alter the κ phase distribution and shape, impacting alloy hardness and wear resistance [10, 11, 20]. The interaction between the κ, α, and β phases can improve the wear characteristics of NAB, making it a popular material for ship propellers and valves. The hardness of NAB depends on microstructural changes produced by forging and heat treatments. Heat treatment can produce phase changes that increase alloy mechanical properties. Equal channel angular pressing and isothermal heat treatment can refine NAB's lamellar structure, increasing hardness [48, 49]. Forging increases hardness, which improves wear resistance for abrasive components [50]. Abrasion resistance is closely connected to hardness. Studies show that harder materials withstand wear better. Studies that indicate wear loss and wear rate decrease with hardness [51 – 53] demonstrate this association.

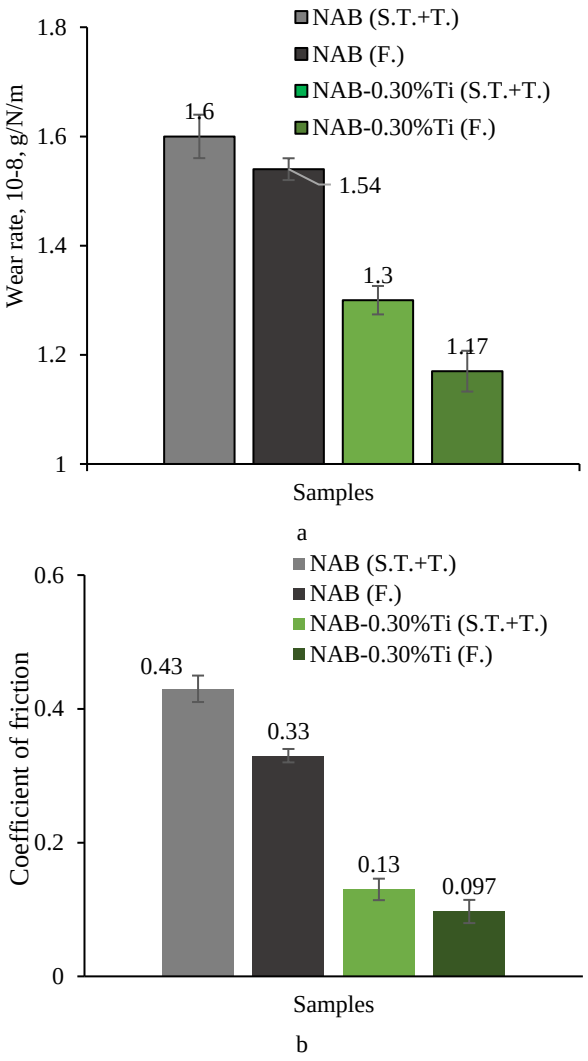

Fig. 6. a – wear rates; b – coefficient of friction of NAB and NAB-0.30%*Ti* alloys after wear tests

The robust intermetallic compound $AlFe_3$ amplifies these phenomena by providing a durable microstructure that resists abrasive wear processes. The size and distribution of hard phases like $AlFe_3$ significantly impact the material's abrasive wear [51]. Material phase composition might also affect wear processes. $AlFe_3$ can change wear from abrasive to sticky depending on loading and counter surface contact [54]. Mechanical features of the AlNi inter-metallic phase include excellent hardness and wear resistance [55]. Wear and friction characteristics have improved using AlNi intermetallic phases [56]. Microstructural development of AlNi phase alloys can significantly affect tribological performance. The coarsening of AlNi precipitates after heat treatment reduces wear resistance, underscoring the importance of microstructural control in mechanical property preservation [57]. Intermetallic phase hardness, especially in high entropy alloys, determines wear behaviour [58]. Materials with the $AlCu_4$ phase are hard because of strengthening processes caused by intermetallic compounds formed during solidification and heat treatments. Hard phases like $AlCu_4$ can block dislocation

migration, making the alloy harder. This is important for wear resistance, as harder materials wear less in hostile situations. Phase composition and production methods affect these alloys' hardness, which affects wear performance [47]. Multiple methods can increase the wear resistance of $AlCu_4$ phase aluminium alloys. Anti-wear intermetallic phases reduce material loss during tribological interactions. Adding a hard phase to the matrix protects against abrasive wear, increasing wear resistance. Titanium improves nickel-aluminium bronze (NAB) alloy hardness and wear resistance, which are crucial for marine and other harsh settings. Titanium is an alloying agent that refines NAB's microstructure and mechanics. Also addressed is the microstructural development of NAB alloys with titanium additions. Titanium helps optimize the microstructure by uniformizing phase distribution, enhancing mechanical properties such as hardness and wear resistance [5, 11]. Through careful alloying material and processing procedures such as heat treatment and deformation, NAB's mechanical characteristics may be greatly improved [11, 59]. Titanium's ability to form intermetallic compounds with aluminium, such AlTi, increases NAB's hardness and strength. Titanium increases alloy hardness and wear resistance. Research shows that titanium refines microstructure, improving mechanical characteristics [12]. The AlTi phase makes many materials harder and more wear-resistant, notably aluminium alloys and coatings. The AlTi phase reduced friction, a key wear resistance factor [60]. Hardness reduces wear, underlining the AlTi phase's role in enhancing these properties [52, 61, 62].

Nickel aluminium bronze (NAB) alloys' tribological performance depends on their coefficient of friction (COF), especially in marine applications where wear resistance and endurance are vital. The coefficient of friction impacts material wear and mechanical system performance. Numerous studies have demonstrated that surface treatments, load conditions, and environmental factors affect NAB coefficient of friction (COF) [21]. Increasing the wear resistance and coefficient of friction of nickel-containing aluminium bronzes shows how alloy composition affects tribological parameters [12]. Titanium in nickel aluminium bronze (NAB) significantly impacts its tribological properties, especially its friction coefficient. Titanium's high strength-to-weight ratio and corrosion resistance can improve bronze alloy performance in various applications, especially in marine environments where NAB is used due to its corrosion and wear resistance [19]. Titanium in NAB may change the microstructure and friction coefficient, according to research. Titanium improves bronze grain structure, increasing hardness and wear resistance [63]. As smaller grains distribute stress more uniformly across contact surfaces, this refinement may reduce the friction coefficient due to increased surface area and load distribution. Titanium's mechanical properties, such as its ability to withstand heavy loads without deformation, may also improve friction coefficient stability under various operational conditions [64]. Friction stir processing increases titanium dispersion in the bronze matrix, improving wear resistance and lowering friction coefficients [25].

Fig. 7 a and b shows the SEM images of NAB and NAB-0.30% Ti alloys after solution treatment (S.T.) and tempering (T) after casting, while Fig. 7 c and d shows the SEM images after forging. Table 3 shows the EDX analysis at the points defined by the morphologies (1-6) in Fig. 7. SEM micrographs exhibit abrasive and adhesive wear mechanisms. Wear micrographs show that plastic deformation causes debris transfer to the surface and wear grooves of different intensities. In addition, two- and three-body interactions caused wear. NAB and NAB-0.30 % Ti alloys after forging (Fig. 7 c and d) generally have debris transfer to the material surface due to adhesive wear. In addition, grooves formed on the wear surface caused the adhesive layer to break and detach.

Table 3. EDX weight percentages of the marked numbers on Fig. 7

	Points	C	O	Al	Ti	Mn	Fe	Ni	Cu
Fig. 7 a and b	1	3.63	3.59	7.12	–	0.12	2.77	6.45	76.33
	2	3.91	5.24	6.46	–	0.66	2.43	5.68	75.62
	3	4.26	4.00	6.92	–	0.01	1.40	6.23	77.20
	4	5.07	0.96	8.66	3.26	–	–	7.17	74.89
	5	5.30	5.40	6.69	5.45	–	0.97	6.06	70.13
	6	5.32	4.87	7.09	4.70	0.39	1.68	5.92	70.04
Fig. 7 c and d	1	4.39	1.41	7.64	–	0.32	1.09	6.96	78.22
	2	4.44	5.01	7.26	–	0.59	1.62	6.57	74.52
	3	4.34	4.94	6.78	–	–	1.02	6.38	76.57
	4	3.86	1.47	7.51	7.17	0.71	2.60	6.51	70.18
	5	5.18	5.66	6.87	7.07	0.37	1.71	5.99	67.20
	6	4.99	1.65	7.41	5.45	0.56	3.06	6.17	70.71

NAB alloy wear scars are deep post solution treatment (S.T.) and tempering (T) following casting and forging. The wear scars show a transformation from abrasive to adhesive character as titanium is added. During solution treatment (S.T.) and tempering (T) in aged NAB alloy, mechanical actions at point 1 in Fig. 7 a cause wear debris to adhere to the wear scars. Point 2 shows that they wear separates particles and create grooves on the surface of the material. In point 3, there are burr-like fragments and wear scars that are not sharper than point 2. In point 4 in Fig. 7 b, small circular fragments adhere to the wear scars at medium depth in aged NAB-0.30 %Ti alloy after solution treatment (S.T.) and tempering (T). In point 5, the scenario is similar to point 1. In point 6, wear scars at medium depth show shell-like and small triangular fragments adhered to the matrix. In Fig. 7 c, a small elliptical fragment separated from the worn NAB alloy after forging is adhered to the surface within the obvious wear scar. In point 2, coarse debris adheres to the matrix. At point 3, there are small spherical fragments in and around the deep channels. In Fig. 7 d, the NAB-0.30 %Ti alloy worn after forging has short, line-like fragments adhering to the extremely fine wear scars at point 4. At point 5, small debris clusters adhere to the matrix. At point 6, small fragments and shells adhere to the moss-like surface. EDX analyses of the worn surface of NAB with 0.3 %Ti addition (points 4, 5 and 6 in Table 3) showed partly some oxide formation. Partially oxygen-rich surface formation, increase in Ti content and increase in hardness led to a decrease in wear rate (Fig. 4).

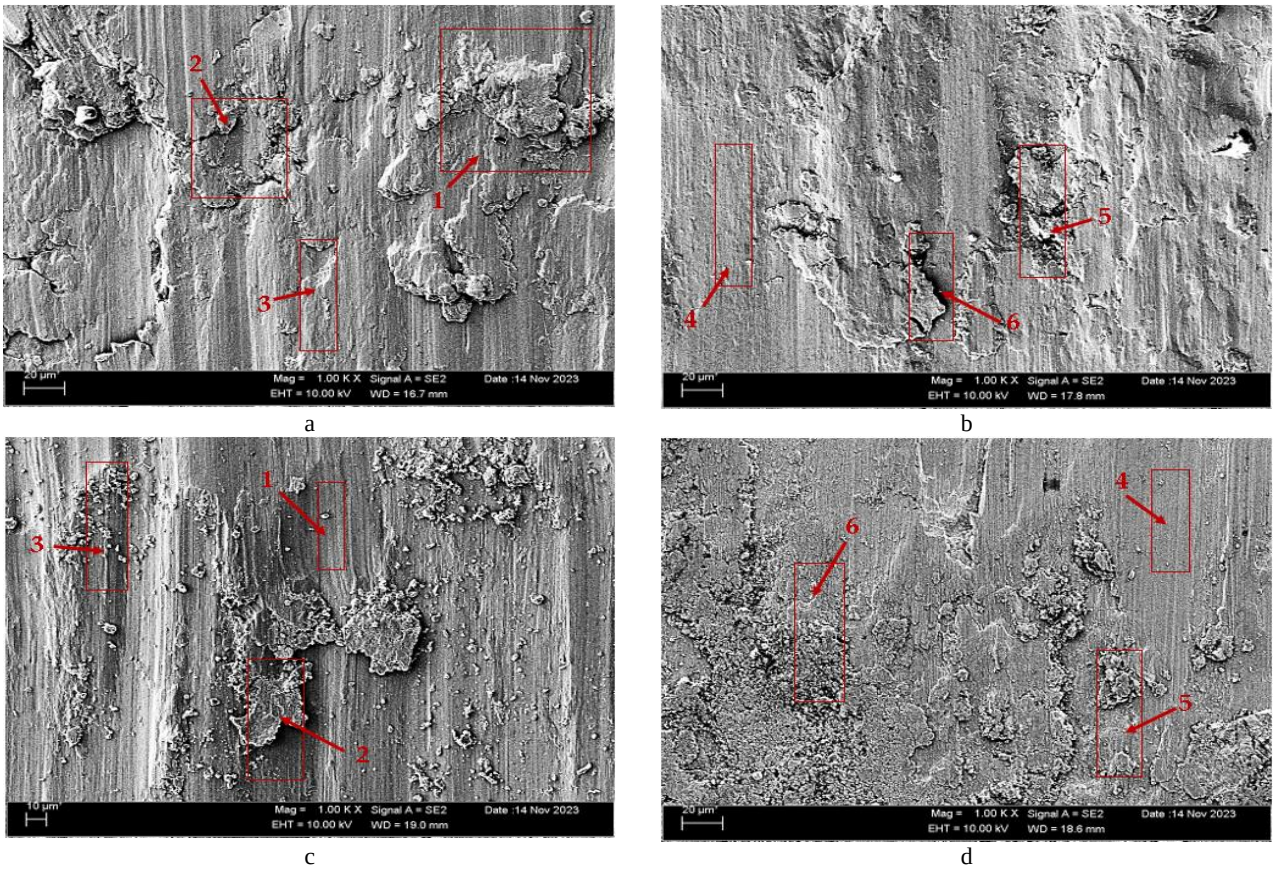

Fig. 7. SEM images of the worn surfaces: after S.T. + T.: a – NAB; b – NAB-0.30 %Ti; c – NAB after F; d – NAB-0.30%Ti after F

4. CONCLUSIONS

After casting, solution treatment and tempering and forging were examined on the tribological characteristics of 0.30 %Ti added NAB. The results are:

1. Heat-treated NAB contains a copper-rich α solid solution phase, martensitic β phase, and intermetallic κ phases. The addition of 0.30 %Ti to NAB led to a more refined and homogeneous grain structure by increasing the number of nucleation sites during solidification. Heat treatment processes, including solution treatment and tempering, facilitated partial decomposition of the martensitic β phase into α and intermetallic phases, further improving microstructural balance. Forging enhanced the microstructure by breaking down dendritic arms into nearly spherical forms and increasing the precipitation of intermetallic κ phases.
2. Hardness of NAB is influenced by microstructural phases: α, β, and κ. Titanium promoted the formation of intermetallic κ phases, which contributed to the stability and increase in hardness. After solution treatment (S.T.) and tempering (T) post-casting and forging (F.), the NAB-0.30 %Ti alloy had the greatest hardness values of 239.53 HB and 254.06 HB, respectively.
3. The combination of titanium alloying improved the hardness and wear resistance of the alloy by enhancing dislocation density, grain boundary strength, and phase uniformity. Overall, the NAB-0.30 %Ti alloy exhibited supe-rior structural integrity and tribological performance compared to the titanium-free NAB alloy, making it a promising candidate for applications requiring high wear resistance. After forging (F.), the NAB-0.30 %Ti alloy showed 0.0035 g weight loss, 1.17×10^{-8} g/N·m wear rate, and 0.097 friction coefficient after 10,000 m of sliding distance.

REFERENCES

1. **Song, Z., Tegus, O.** The Corrosion Properties of Bronze Alloys in NaCl Solutions *Materials* 16 2023: pp. 5144. https://doi.org/10.3390/ma16145144
2. **Scudino, S., Unterdoerfer, C., Prashanth, K.G., Attar, H., Ellendt, N., Uhlenwinkel, V., Eckert, J.** Additive Manufacturing of Cu-10Sn Bronze *Materials Letters* 156 2015: pp. 202 – 204. https://doi.org/10.1016/j.matlet.2015.05.076
3. **Zhao, X., Qi, Y., Wang, J., Peng, T., Zhang, Z., Li, K.** Effect of Weld and Surface Defects on the Corrosion Behavior of Nickel Aluminum Bronze in 3.5% NaCl Solution *Metals* 10 2020: pp. 1227. https://doi.org/10.3390/met10091227
4. **Fang, J., Song, G., Liu, W., Li, Q.** Microstructure Evolution of As-Cast Nickel Aluminum Bronze under Electropulsing *Key Engineering Materials* 861 2020: pp. 28 – 34. https://doi.org/10.4028/www.scientific.net/KEM.861.28
5. **Thossatheppitak, B., Suranuntchai, S., Uthaisangsuk, V., Manonukul, A., Mungsantisuk, P.** Microstructure Evolution of Nickel Aluminum Bronze Alloy during Compression at Elevated Temperatures *Advanced Materials Research* 893 2014: pp. 365 – 370. https://doi.org/10.4028/www.scientific.net/AMR.893.365

6. **Iannuzzi, M.; Vasanth, K.; Frankel, G.** Unusual Correlation between SKPFM and Corrosion of Nickel Aluminum Bronzes *Journal of The Electrochemical Society* 164 2017: pp. C488 – C497. https://doi.org/10.1149/2.0391709jes
7. **Lv, Y., Wang, L., Han, Y., Xu, X., Lu, W.** Investigation of Microstructure and Mechanical Properties of Hot Worked NiAl Bronze Alloy with Different Deformation Degree *Materials Science and Engineering: A* 643 2015: pp. 17 – 24. https://doi.org/10.1016/j.msea.2015.06.078
8. **Anantapong, J., Uthaisangsuk, V., Suranuntchai, S., Manonukul, A.** Effect of Hot Working on Microstructure Evolution of As-Cast Nickel Aluminum Bronze Alloy *Materials & Design* 60 2014: pp. 233 – 243. https://doi.org/10.1016/j.matdes.2014.03.033
9. **Ding, Y., Zhao, R., Qin, Z., Wu, Z., Wang, L., Lei, L., Lu, W.** Evolution of the Corrosion Product Film on Nickel-Aluminum Bronze and Its Corrosion Behavior in 3.5 Wt % NaCl Solution *Materials* 12 2019: pp. 209. https://doi.org/10.3390/ma12020209
10. **Böhm, J., Linhardt, P., Strobl, S., Haubner, R., Biezma, M.** Microstructure of a Heat-Treated Nickel-Aluminum Bronze and Its Corrosion Behavior in Simulated Fresh and Sea Water *Materials Performance and Characterization* 5 2016: pp. 689 – 700. https://doi.org/10.1520/MPC20160029
11. **Wu, Z., Hu, Q., Qin, Z., Zhang, Y., Xia, D.H., Hu, W.** Effect of Plastic Deformation on Mechanical Properties and Corrosion Resistance of Nickel-Aluminum Bronze *Anti-Corrosion Methods and Materials* 68 2021: pp. 473 – 480. https://doi.org/10.1108/ACMM-12-2020-2411
12. **Kulakli, A., Şeşen, F., Çitrak, T., ÖZEREN, T.** Effect of Cobalt and Titanium Additions on Corrosion and Wear Resistance of Nickel Containing Aluminium Bronzes *Conference Metal* 2020: pp. 1135 – 1141. https://doi.org/10.37904/metal.2020.3616
13. **Doğan, Z.E., Kahrıman, F., Atapek, Ş.H.** Microstructural and Thermal Characterization of Aluminum Bronzes *Kocaeli Journal of Science and Engineering* 1 2018: pp. 6 – 10. https://doi.org/10.34088/kojose.405810
14. **Nascimento, M., Santos, G., Teram, R., Torres dos Santos, V., Silva, M., Couto, A.** Effects of Thermal Variables of Solidification on the Microstructure, Hardness, and Microhardness of Cu-Al-Ni-Fe Alloys *Materials* 12 2019: pp. 1267. https://doi.org/10.3390/ma12081267
15. **Tan, Z., Guo, Q., Zhai, W., Zhao, Z.** Tribological Characteristics of Nickel-Aluminium Bronze CuAl10Ni5Fe4 against 30CrMnSiA Steel after the Prior Corrosion Treatment *Applied Mechanics and Materials* 201 – 202 2012: pp. 73 – 77. https://doi.org/10.4028/www.scientific.net/AMM.201-202.73
16. **Lee, S., Kim, K., Choi, W.** Annoyance Caused by Amplitude Modulation of Wind Turbine Noise *Noise Control Engineering Journal* 59 2011: pp. 38 – 46. https://doi.org/10.3397/1.3531797
17. **Ocejo, I., Biezma, M., Linhardt, P.** Corrosion Evaluation of Welded Nickel Aluminum Bronze and Manganese Aluminum Bronze in Synthetic Sea Water *Materials and Corrosion* 73 (11) 2022: pp. 1788 – 1799. https://doi.org/10.1002/maco.202213328
18. **Omotoyinbo, J., Oyetunji, A., Oloruntoba, D.** Quantitative Analysis of Silicon Influence and Deformation Impact on the Mechanical and Corrosion Characteristics of Nickel Aluminium Bronze (NAB) Alloy *FUOYE Journal of Engineering and Technology* 9 2024: pp. 117 – 123. https://doi.org/10.4314/fuoyejet. v9i1.18
19. **Zhang, B.B., Wang, J.Z., Yuan, J.Y., Yan, F.Y.** Tribocorrosion Behavior of Nickel Aluminum Bronze in Seawater: Identification of Corrosion-wear Components and Effect of pH *Materials and Corrosion* 69 2017: pp. 106 – 114. https://doi.org/10.1002/maco.201709648
20. **Anene, F., Nwankwo, N., Nwoke,V.** Effect of Dopant and Heat Treatment on the Microstructure and Mechanical Properties of Nickel-Aluminum Bronze *Metallurgical and Materials Engineering* 25 2019: pp. 147 – 162. https://doi.org/10.30544/423
21. **Chen, C., Yang, Q., Chen, Q., Wang, Y., Xu, D., Li, H., Xiliang, Z., Harvey, C., Liu, J.** Tribological Properties of Copper-Embedded Self-Lubricating Bearing Materials *Industrial Lubrication and Tribology* 74 2022: pp. 796 – 803. https://doi.org/10.1108/ILT-03-2022-0067
22. **Lv, Y., Ding, Y., Han, Y., Zhang, L.C., Wang, L., Lu, W.** Strengthening Mechanism of Friction Stir Processed and Post Heat Treated NiAl Bronze Alloy: Effect of Rotation Rates *Materials Science and Engineering: A* 685 2017: pp. 439 – 446. https://doi.org/10.1016/j.msea.2016.12.050
23. **Xu, X., Lv, Y., Hu, M., Xiong, D., Zhang, L., Wang, L., Lu, W.** Influence of Second Phases on Fatigue Crack Growth Behavior of Nickel Aluminum Bronze *International Journal of Fatigue* 82 2016: pp. 579 – 587. https://doi.org/10.1016/j.ijfatigue.2015.09.014
24. **Wu, Z., Cheng, Y., Lei, L., Lv, W., Hu, W.** Effect of Heat Treatment on Microstructure Evolution and Erosion-Corrosion Behavior of a Nickel-Aluminum Bronze Alloy in Chloride Solution *Corrosion Science* 98 2015: pp. 260 – 270. https://doi.org/10.1016/j.corsci.2015.05.037
25. **Khazaei, B., Keshavarz, S.** Nickel-Aluminum-Bronze/Al_2O_3 Surface Nanocomposite Produced by Friction-Stir Processing: Corrosion Properties and Microstructure *Materials and Corrosion* 68 2017: pp. 883 – 891. https://doi.org/10.1002/maco.201609369
26. **Yang, L., Wei, Y.** Corrosion Evolution of Nickel Aluminum Bronze in Clean and Sulfide-Polluted Solutions *Coatings* 13 2023: pp. 846. https://doi.org/10.3390/coatings13050846
27. **Jin, K., Qiao, Z., Wang, S., Zhu, S., Cheng, J., Yang, J., Liu, W.** The Effects of Main Components of Seawater on the Tribological Properties of Cu-9Al-5Ni-4Fe-Mn Alloy Sliding against AISI 52100 Steel *RSC Advances* 6 2016: pp. 6384 – 6394. https://doi.org/10.1039/C5RA19719H
28. **Chen, Z., Sun, X., Huang, Y.** A Brief Discussion about Nickel Aluminum Bronze Propeller Failure Modes and Its Repair Methods *Key Engineering Materials* 723 2016: pp. 125 – 129. https://doi.org/10.4028/www.scientific.net/KEM.723.125
29. **Chen, Q., Zhang, Z., Qi, Y.** Effect of Composite Epoxy Coating on Protective and Bonding Properties to Nickel Aluminum Bronze *Advanced Engineering Materials* 25 2022: pp. 1326. https://doi.org/10.1002/adem.202201326

30. **Qin, Z., Zhang, Q., Luo, Q., Wu, Z., Shen, B., Lei, L., Hu, W.** Microstructure Design to Improve the Corrosion and Cavitation Corrosion Resistance of a Nickel-Aluminum Bronze *Corrosion Science* 139 2018: pp. 255 – 266. https://doi.org/10.1016/j.corsci.2018.04.043
31. S**un Guo, Q., Sun, Y., Yong Hua, D.** Structure and Properties of W-Ti Thin Films Deposited by Magnetron Sputtering *Materials Science Forum* 849 2016: pp. 654. https://doi.org/10.4028/www.scientific.net/msf.849.654
32. **Schuetzke, J., Schweidler, S., Münke, F., Orth, A., Khandelwal, A., Breitung, B., Aghassi-Hagmann, J., Reischl, M.** Accelerating Materials Discovery: Automated Identification of Prospects from X-Ray Diffraction Data in Fast Screening Experiments *Advanced Intelligent Systems* 6 2023: pp. 501. https://doi.org/10.1002/aisy.202300501
33. **Nová, I., Machuta, J., Raur, L.** The Influence of Microalloying on the Thermal Treatment of Aluminum Bronzes *Manufacturing Technology* 17 2017: pp. 797 – 804. https://doi.org/10.21062/ujep/x.2017/a/1213-2489/MT/17/5/797
34. **Öztürk, S., Sünbül, S., Metoğlu, A., Önal, S., İcin, K.** Characterisation of Nickel–Aluminium Bronze Powders Produced by the Planar Flow Casting Method *Materials Science and Technology* 36 2020: pp. 1771 – 1784. https://doi.org/10.1080/02670836.2020.1834681
35. **Yaseen, M., Mansoor, M., Ansari, H., Hussain, S., Khan, S.** Effect of Heat Treatment on Tribological Characteristics of CuAl10Ni5Fe4 Nickel Aluminum Bronze *Key Engineering Materials* 778 2018: pp. 61 – 67. https://doi.org/10.4028/www.scientific.net/KEM.778.61
36. **Ding, Y., Lv, Y., Chen, K., Zhao, B., Han, Y., Wang, L., Lu, W.** Effects of Microstructure on the Stress Corrosion Cracking Behavior of Nickel-Aluminum Bronze Alloy in 3.5% NaCl Solution *Materials Science and Engineering: A* 733 2018: pp. 361 – 373. https://doi.org/10.1016/j.msea.2018.07.066
37. **Hårsta, A., Rundqvist, S.** The Crystal Chemistry of Kappa-Phases *Journal of Solid-State Chemistry* 70 1987: pp. 210 – 218. https://doi.org/10.1016/0022-4596(87)90058-2
38. **Pisarek, B.** Model of Cu-Al-Fe-Ni Bronze Crystallization *Archives of Foundry Engineering* 14 2013: pp. 39 – 44. https://doi.org/10.2478/afe-2013-0063
39. **Wharton, J., Stokes, K.** The Influence of Nickel–Aluminium Bronze Microstructure and Crevice Solution on the Initiation of Crevice Corrosion *Electrochimica Acta* 53 2008: pp. 2463 – 2473. https://doi.org/10.1016/j.electacta.2007.10.047
40. **Nabach, W.** The Effects of Isothermal Deformation and Annealing on the Microstructure of Nickel-Aluminium-Bronze Propeller Material. PhD Thesis, Naval Postgraduate School 2003: pp. 63.
41. **Barik, R., Wharton, J., Wood, R., Stokes, K.** Nickel-Aluminium Bronze Pitting Corrosion in Seawater Environment and Mitigation; January 1 2009; Conference: Maritime studies launch event. At: University of Southampton.
42. **Zheng, J., Liu, R., Ning, L.** Selective Corrosion of Cast Nickel–Aluminum Bronze in Seawater *Materials and Corrosion* 74 2022: pp. 364 – 372. https://doi.org/10.1002/maco.202213482
43. **Maximov, J., Duncheva, G., Anchev, A., Dunchev, V., Argirov, Y., Todorov, V., Mechkarova, T.** Effects of Heat Treatment and Severe Surface Plastic Deformation on Mechanical Characteristics, Fatigue, and Wear of Cu-10Al-5Fe Bronze *Materials* 15 2022: pp. 8905. https://doi.org/10.3390/ma15248905
44. **Segun, B., Chukwulozie, O., Adeleye, S.** Effect of Tin Addition on the Mechanical Properties and Microstructure of Aluminium Bronze Alloyed with 4% Nickel *European Journal of Theoretical and Applied Sciences* 2 2024: pp. 3 – 17. https://doi.org/10.59324/ejtas.2024.2(3).01
45. **Oluwadare, B.S., Adebayo, A., Stephen, J.T.** The Influence of the Addition of Nickel on the Structure and Mechanical Properties of Aluminium Bronze Alloy *Review of Industrial Engineering Letters* 5 2019: pp. 12 – 21. https://doi.org/10.18488/journal.71/2019.51.12.21
46. **Adamiak, M., Appiah, A., Woźniak, A., Nuckowski, P., Nazarov, S., Ganiev, I.** Impact of Titanium Addition on Microstructure, Corrosion Resistance, and Hardness of As-Cast Al+6%Li Alloy *Materials* 16 2023: pp. 2671. https://doi.org/10.3390/ma16072671
49. **Çetin, T., Akkaş, M.** Effect of WC Reinforced on Microstructure and Mechanical Properties of CuAlMn Alloys Produced By Hot Pressing Method *European Journal of Technic* 2020: pp. 173 – 183. https://doi.org/10.36222/ejt.697601
48. **Barr, C., McDonald, D., Xia, K.** Significantly Enhanced Tensile Strength and Ductility in Nickel Aluminium Bronze by Equal Channel Angular Pressing and Subsequent Heat Treatment *Journal of Materials Science* 48 2013: pp. 4749 – 4757. https://doi.org/10.1007/s10853-013-7256-2
49. **Dutta, V., Thakur, L., Singh, B., Vasudev, H.** A Study of Erosion–Corrosion Behaviour of Friction Stir-Processed Chromium-Reinforced NiAl Bronze Composite *Materials* 15 2022: pp. 5401. https://doi.org/10.3390/ma15155401
50. **Berlanga-Labari, C., Claver, A., Biezma, M., Fernandez Palacio, J.** Study of Effect of Nickel Content on Tribocorrosion Behaviour of Nickel–Aluminium–Bronzes (NABs) *Lubricants* 11 2023: pp. 43. https://doi.org/10.3390/lubricants11020043
51. **Rodinger, T., Lukšić, H., Ćorić, D., Rede, V.** Abrasion Wear Resistance of Precipitation-Hardened Al-Zn-Mg Alloy *Materials* 17 2024: pp. 2446. https://doi.org/10.3390/ma17102446
52. **Zhang, X., Xu, J., He, W., Jia, J.** Effect of Multidirectional Forging and Aging Treatment on Wear Properties of ZK61 Alloy *Materials* 17 2024: pp. 523. https://doi.org/10.3390/ma17020523
53. **Jha, A.K., Gachake, A., Prasad, B.K., Dasgupta, R., Singh, M., Yegneswaran, A.H.** High Stress Abrasive Wear Behavior of Some Hardfaced Surfaces Produced by Thermal Spraying *Journal of Materials Engineering and Performance* 11 2002: pp. 37 – 45. https://doi.org/10.1007/s11665-002-0006-2
54. **Kumar Gatenda, C., Liu, Y., Zhu, W.** Effect of W Content on Wear Resistance of CoCrFeNiMnWx High Entropy Alloy. In Proceedings of the Smart Manufacturing and Material Processing (SMMP) *Volkson Press* 2023: pp. 37 – 40. https://doi.org/10.26480/smmp.01.2023.37.40
55. **Tang, S., Li, Y., Gao, Y., Zheng, Q., Liu, Z., Ren, X.** First-Principles Investigations of the Structural, Anisotropic Mechanical, Thermodynamic and Electronic Properties of the $AlNi_2Ti$ Compound *Crystals* 8 2018: pp. 93. https://doi.org/10.3390/cryst8020093

56. **Jainulabdeen, A., Ramanathan, S., Vinoth, S., Ganesan, V., Priyadharshini, S., Krishnakumar, K.** Studies on Microstructural Evolution and Wear Behaviour of AlNi Intermetallic Reinforced AA6061 Alloy in T6 Conditio *Archives of Metallurgy and Materials* 2021: pp. 803 – 813. https://doi.org/10.24425/amm.2022.139670
57. **Yan, D., Shi, C., Wang, J., Zhang, Y., Sun, J., Wang, Y., Liu, P.** Microstructure and Properties of Laser Cladding AlxFeCoCrNiMn High Entropy Alloy of Q345 Steel *Materials Research* 26 2023: pp. 154. https://doi.org/10.1590/1980-5373-mr-2022-0154
58. **Ayyagari, A., Hasannaeimi, V., Grewal, H., Arora, H., Mukherjee, S.** Corrosion, Erosion and Wear Behavior of Complex Concentrated Alloys: A Review *Metals* 8 2018: pp. 603. https://doi.org/10.3390/met8080603
59. **Novák, P., Barták, Z., Nová, K., Průša, F.** Effect of Nickel and Titanium on Properties of Fe-Al-Si Alloy Prepared by Mechanical Alloying and Spark Plasma Sintering *Materials* 13 2020: pp. 800. https://doi.org/10.3390/ma13030800
60. **Gordilloh, O., Hincapie Campos, W., Piamba, O., Olaya, J., Trava-Airoldi, V.** Study of Adhesive Wear Test on TiSi, AlTi, and WTi Coatings *Coatings* 12 2022: pp. 1370. https://doi.org/10.3390/coatings12101370
61. **Kohlscheen, J., Bareiss, C.** Effect of Hexagonal Phase Content on Wear Behaviour of AlTiN Arc PVD Coatings *Coatings* 8 2018: pp. 72. https://doi.org/10.3390/coatings8020072
62. **Kadhim, D., Koricherla, M.V., Scharf, T.** Room and Elevated Temperature Sliding Friction and Wear Behavior of Al0.3CoFeCrNi and Al0.3CuFeCrNi2 High Entropy Alloys *Crystals* 13 2023: pp. 609. https://doi.org/10.3390/cryst13040609
63. **Kozana, J., Garbacz-Klempka, A., Piękoś, M., Perek-Nowak, M., Pałka, P.** Experimental Investigation and Thermodynamic Modeling of Influence of Nickel and Titanium Content on the Structure and Selected Properties of Tin Bronzes *Materials* 14 2021: pp. 5944. https://doi.org/10.3390/ma14205944
64. **Morales, J., Piamba, O., Olaya, J., Vallejo, F.** Effect of Heat Treatment on the Electrochemical and Tribological Properties of Aluminum-Bronze Coatings Deposited Used the Thermal Spraying Process *Coatings* 14 2024: pp. 423. https://doi.org/10.3390/coatings14040423